IEEE Access
Multidisciplinary | Rapid Review | Open Access Journal

Received 24 March 2024, accepted 18 April 2024, date of publication 25 April 2024, date of current version 3 May 2024.

Digital Object Identifier 10.1109/ACCESS.2024.3393836

RESEARCH ARTICLE

A Lowpass-Bandpass Triplexer With A New Microstrip Configuration and Compact Size for 5G and Energy Harvesting Applications

SALAH I. YAHYA[1], (Senior Member, IEEE), FARID ZUBIR[2], (Member, IEEE), LEWIS NKENYEREYE[3], MOHAMMED ABDEL HAFEZ[4], (Senior Member, IEEE), LEILA NOURI[5,6], MAHER ASSAAD[7], MUHAMMAD AKMAL CHAUDHARY[7], (Senior Member, IEEE), AND NOORLINDAWATY MD. JIZAT[8], (Member, IEEE)

[1]Department of Communication and Computer Engineering, Cihan University-Erbil, Erbil 0383-23, Iraq
[2]Wireless Communication Centre, Faculty of Electrical Engineering, Universiti Teknologi Malaysia, Johor Bahru, Johor 81310, Malaysia
[3]Department of Computer and Information Security, Sejong University, Seoul 05006, South Korea
[4]Department of Electrical and Communication Engineering, United Arab Emirates University, Al Ain, United Arab Emirates
[5]Institute of Research and Development, Duy Tan University, Da Nang 550000, Vietnam
[6]School of Engineering and Technology, Duy Tan University, Da Nang 550000, Vietnam
[7]Department of Electrical and Computer Engineering, College of Engineering and Information Technology, Ajman University, Ajman, United Arab Emirates
[8]Faculty of Engineering, Multimedia University, Cyberjaya, Selangor 63100, Malaysia

Corresponding authors: Farid Zubir (faridzubir@utm.my), Lewis Nkenyereye (nkenyele@sejong.ac.kr), Leila Nouri (leilanouri@duytan.edu.vn), and Noorlindawaty Md. Jizat (noorlindawaty.jizat@mmu.edu.my)

This work was supported in part by the Higher Institution Centre of Excellence (HICOE), Ministry of Higher Education Malaysia through the Wireless Communication Centre (WCC), Universiti Teknologi Malaysia (UTM), under Grant A.J091300.6800.09465 and Grant R.J090301.7823.4J610; and in part by the Faculty of Engineering, Multimedia University (MMU), Cyberjaya, Selangor, Malaysia.

ABSTRACT This research presents a novel microstrip configuration for a lowpass-bandpass triplexer. To design this triplexer, first a lowpass filter (LPF) with some empty spaces is designed. Then, two microstrip sections are embedded inside the empty spaces to create bandpass (BP) channels. Therefore, this triplexer occupies a very small size of 0.003 λg^2. A rigorous mathematical analysis and an optimization process are conducted to enhance the triplexer performance. The proposed triplexer features a lowpass (LP) channel cut-off frequency at 870 MHz with bandpass (BP) channels operating at 1.335 GHz and 2.055 GHz. The achieved insertion losses are 0.2 dB, 0.09 dB, and 0.04 dB for all LP and BP channels that are remarkably low, making our triplexer ideal for energy harvesting applications. All bands are flat with suitable group delays (GDs). Meanwhile, the BP channels are wide with 14.1% and 25.5% fractional bandwidths (FBWs) for the middle and upper channels respectively. Our triplexer suppresses the harmonics after the LP channel from the 1st harmonic up to 3rdharmonic. Fabrication and measurement of the proposed triplexer validate our designing method and the simulation results.

INDEX TERMS Microstrip, triplexer, 5G, lowpass-bandpass, energy harvesting.

I. INTRODUCTION

Microstrip structures are a suitable choice for creating filters, diplexers, triplexers and other passive filtering devices [1], [2], [3], [4], [5], [6]. Among them, the devices with multiple channels are less suggested. Lowpass-bandpass (LP-BP) filtering devices are more complex compared to bandpass (BP) devices as they require designing both lowpass (LP) and bandpass cells. In contrast, BP devices only need a mid-band resonator. Consequently, microstrip LP-BP triplexers [6], [7], [8], [9], [10] are not frequently reported in the literature.

All of the reported microstrip LP-BP triplexers in [6], [7], [8], [9], and [10] have large sizes. The proposed triplexer in [6] is suitable for GSM and 5G applications, which

The associate editor coordinating the review of this manuscript and approving it for publication was Ali Karami Horestani.

has low group delays (GDs) at all its bands. In [7], the microstrip T-shape stubs are used to obtain a balun-integrated LP-BP triplexer. In [8] coupled hairpin and coupled U-shape cells are utilized to improve the isolation of a LP-BP triplexer. However, this triplexer has high losses. The LP-BP triplexer in [9], is designed based on integrating the interdigital microstrip cells. But it has high losses at the 2nd and 3rd channels. The designers in [10] could reduce the size in comparison to the other microstrip LP-BP triplexers. However, it seems that by using new configurations, the size can be reduced again. Some microstrip bandpass-bandpass (BP-BP) triplexers with large sizes are introduced in [11], [12], [13], and [14]. Simple stub loaded coupled lines in [11], complex microstrip meandrous lines in [12], multimode net-type resonators in [13] and the simple open loops in [14] have been used. All of these BP-BP triplexers have high insertion losses while none of them could increase the fractional bandwidth (FBW) to 10%. Four LP-BP diplexers are achieved based on various microstrip structures in [15], [16], [17], and [18]. Similar to most of triplexers they have large dimensions. This is while usually a diplexer can occupy less size than a triplexer. Some of these diplexers and triplexers did not pay attention to improve group delay (GD). Because designing of these filtering passive devices are harder than common filters. On the other hand, some passive microstrip devices in [19], [20], [21], [22], [23], and [24] tried to improve the group delay. However, they could not achieve the desired results.

This work aims to develop an ultra-compact LP-BP triplexer using an innovative microstrip configuration tailored for optimal performance in 5G applications. Key objectives include minimizing group delay and losses while ensuring efficient operation across the target frequency range. The design process involves comprehensive mathematical analysis to predict the behavior of a fundamental structure, facilitating streamlined optimization and dimension determination. Following the design phase, the proposed triplexer will undergo rigorous simulation and measurement procedures to validate its performance. Comparative analysis with existing literature will be conducted to highlight the distinctive advantages of the proposed triplexer, highlighting its potential for enhancing signal processing capabilities in advanced communication systems. This triplexer has practical applications in various communication systems and RF devices where multiple frequency bands need to be separated or combined efficiently such as cellular, Wi-Fi, and satellite communication.

II. DESIGN PROCESS

To achieve a LP-BP triplexer, two BPFs and one LPF filter are needed. Traditional methods of designing diplexers and triplexers focus on separate design of filters. Then they are connected with a matching circuit. But we do not use this method for our design. First, we will design a LPF, then coupling structures will be embedded inside the LPF structure to create intermediate bands. Fig.1(a) depicts the basic layout

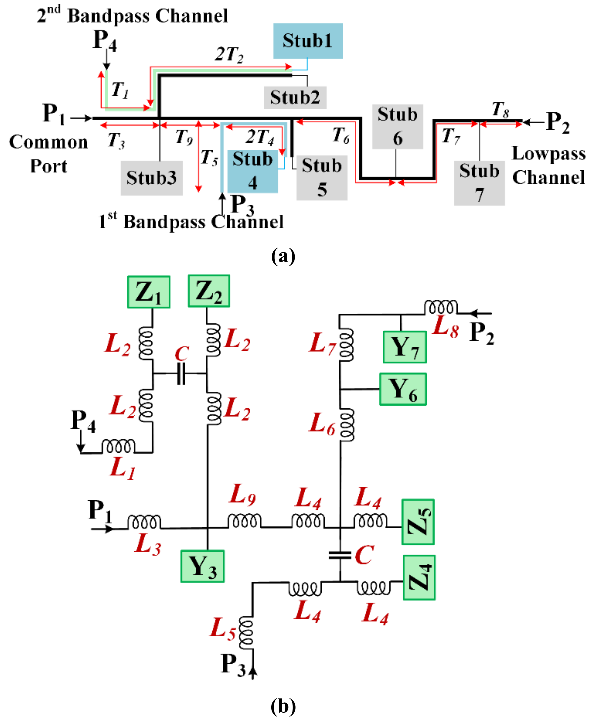

FIGURE 1. LP-BP triplexer design (a) basic semi-layout, (b) approximated LC model.

of our LP-BP triplexer. The LP channel will be created at port 2 (P_2), where port 1 (P_1) is the common port. The BP channels will be produced through P_1, P_3 (middle channel) and P_1, P_4 (upper channel). In order to obtain the LP channel Stubs 2, 3, 5, 6 and 7 are loaded on a long thin microstrip transmission line (TL). The Stubs 1 and 4 are added for improving the performance of the BP channels. However, the loading effects of them on the LP channel cannot be ignored. For analyzing this structure, its approximated LC model is presented in Fig.1(b). The equivalent of the thin TLs i.e. T_i ($i = 1,2,..,9$) are the inductors L_i ($i = 1,2,..,9$). The coupling effects are presented by the capacitors C. To reach a more precise LC model of the coupled lines, the number of capacitors should be increased and the transmission lines $2T_2$ and $2T_4$ should be divided into more and smaller inductors. Moreover, in this approximated LC circuit we unnoticed effects of steps and bents. Because they are less important at lower than 10 GHz frequencies. The impedances of the Stubs i ($i = 1,2,4,5$) are Z_i($i = 1,2,4,5$). Also, the admittances of the Stubs 3, 6 and 7 are presented by Y_3, Y_{46} and Y_7 respectively.

For analyzing the LP section, the ports P_3 and P_4 are opened as shown in Fig.2. The admittances Y_8 and Y_9 are calculated as follows:

$$Y_8 = Y_3 + \frac{1}{\frac{1}{\frac{1}{Z_1 + j\omega L_2 + \frac{1}{j\omega C}} + \frac{1}{Z_2 + j\omega L_2}} + j\omega L_2} \tag{1}$$

$$Y_9 = \frac{(Z_4 + j\omega L_4 + \frac{1}{j\omega C})(j\omega L_4 + Z_5)}{Z_4 + 2j\omega L_4 + \frac{1}{j\omega C} + Z_5} \tag{2}$$

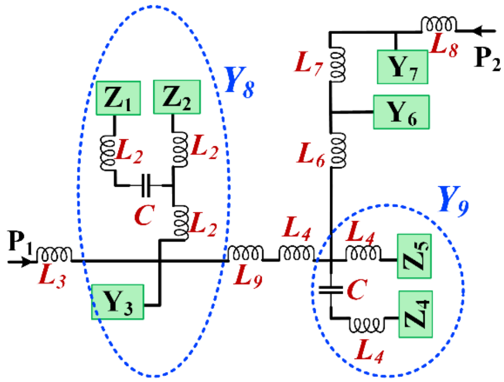

FIGURE 2. **Approximated equivalent LC circuit of the LP cell, where ports 3 and 4 are open.**

The target cut-off frequency, coupling capacitors and inductors are usually in GHz, pF (or fF) and nH ranges, respectively. So, we can calculate the approximated values of Y_8 and Y_9 as follows:

$$Z_1 + j\omega L_2 + \frac{1}{j\omega C} \approx \frac{1}{j\omega C} \rightarrow Y_8 \approx Y_3 + \frac{1}{\frac{1}{\frac{1}{\frac{1}{j\omega C}} + \frac{1}{Z_2 + j\omega L_2}} + j\omega L_2} \tag{3}$$

$$\begin{cases} Z_4 + j\omega L_4 + \frac{1}{j\omega C} \approx Z_4 + \frac{1}{j\omega C} \\ Z_4 + 2j\omega L_4 + \frac{1}{j\omega C} + Z_5 \approx Z_4 + \frac{1}{j\omega C} + Z_5 \end{cases} \rightarrow$$
$$Y_9 \approx \frac{(Z_4 + \frac{1}{j\omega C})(j\omega L_4 + Z_5)}{Z_4 + \frac{1}{j\omega C} + Z_5} \tag{4}$$

For analyzing the approximated equivalent LC circuit of the LP cell, we can calculate the *ABCD* matrix of it. This matrix named as M_{12} and can be obtained as follows:

$$M_{12} = \begin{bmatrix} A_1 & B_1 \\ C_1 & D_1 \end{bmatrix} = \begin{bmatrix} 1 & j\omega L_3 \\ 0 & 1 \end{bmatrix} \times \begin{bmatrix} 1 & 0 \\ Y_8 & 1 \end{bmatrix} \times \begin{bmatrix} 1 & j\omega(L_4+L_9) \\ 0 & 1 \end{bmatrix} \times \begin{bmatrix} 1 & 0 \\ Y_9 & 1 \end{bmatrix} \times \begin{bmatrix} 1 & j\omega L_6 \\ 0 & 1 \end{bmatrix} \times \begin{bmatrix} 1 & 0 \\ Y_6 & 1 \end{bmatrix} \times \begin{bmatrix} 1 & j\omega L_7 \\ 0 & 1 \end{bmatrix} \times \begin{bmatrix} 1 & 0 \\ Y_7 & 1 \end{bmatrix} \times \begin{bmatrix} 1 & j\omega L_8 \\ 0 & 1 \end{bmatrix} \tag{5}$$

If the impedances of Stubs 2, 4, 5, 6 and 7 are low and the impedance of Stub 3 is high, then the admittances Y_8 and Y_9 and M_{12} matrix will be shortened as follows:

$$\begin{cases} Y_8 \approx \frac{1}{\frac{1}{j\omega C + \frac{1}{j\omega L_2}} + j\omega L_2} \\ j\omega C + \frac{1}{j\omega L_2} \approx \frac{1}{j\omega L_2} \end{cases} \rightarrow Y_8 \approx \frac{1}{2j\omega L_2} \tag{6}$$

$$Y_9 \approx j\omega L_4 \tag{7}$$

$$M_{12} \approx \begin{bmatrix} 1 & j\omega L_3 \\ 0 & 1 \end{bmatrix} \times \begin{bmatrix} 1 & 0 \\ \frac{1}{2j\omega L_2} & 1 \end{bmatrix} \times \begin{bmatrix} 1 & j\omega(L_4+L_9) \\ 0 & 1 \end{bmatrix} \times \begin{bmatrix} 1 & 0 \\ j\omega L_4 & 1 \end{bmatrix} \times \begin{bmatrix} 1 & j\omega L_6 \\ 0 & 1 \end{bmatrix} \times \begin{bmatrix} 1 & 0 \\ Y_6 & 1 \end{bmatrix} \times \begin{bmatrix} 1 & j\omega L_7 \\ 0 & 1 \end{bmatrix} \times \begin{bmatrix} 1 & 0 \\ Y_7 & 1 \end{bmatrix} \times \begin{bmatrix} 1 & j\omega L_8 \\ 0 & 1 \end{bmatrix} \tag{8}$$

After applying the approximation and removing small terms M_{12} is derived as follows:

$$\begin{aligned} M_{12} &= \begin{bmatrix} A_1 & B_1 \\ C_1 & D_1 \end{bmatrix} \approx \begin{bmatrix} K_0 & j\omega K_1 \\ \frac{1}{2j\omega L_2} & K_2 \end{bmatrix} \\ &\times \begin{bmatrix} 1 & j\omega L_6 \\ j\omega L_4 & -\omega^2 L_4 L_6 \end{bmatrix} \\ &\times \begin{bmatrix} j\omega L_7 Y_7 & -\omega^2 L_7 L_8 Y_7 \\ j\omega L_7 Y_7 Y_6 & -\omega^2 L_7^2 Y_6^2 \end{bmatrix} \rightarrow \\ A_1 &\approx j\omega L_7 Y_7 [K_0 - \omega^2 L_4 K_1] \\ &\quad - \omega^2 L_7 Y_7 Y_6 L_6 (K_0 - \omega^2 L_4 K_1) \\ B_1 &\approx -\omega^2 L_7 L_8 Y_7 (K_0 - \omega^2 L_4 K_1) \\ &\quad - \omega^2 L_7^2 Y_6^2 j\omega L_6 (K_0 - \omega^2 L_4 K_1) \\ C_1 &\approx (\frac{L_7 Y_7}{2L_2} - \omega^2 L_7 Y_7 L_4 K_2) \\ &\quad + j\omega L_7 Y_7 Y_6 (\frac{L_6}{2L_2} - \omega^2 L_4 L_6 K_2) \\ D_1 &\approx -\omega^2 L_7 L_8 Y_7 (\frac{1}{2j\omega L_2} + j\omega L_4 K_2) \\ &\quad - \omega^2 L_7^2 Y_6^2 (\frac{L_6}{2L_2} - \omega^2 L_4 L_6 K_2) \\ K_0 &= 1 + \frac{L_3}{2L_2} \\ K_1 &= L_3 + (L_4 + L_9) K_0 \\ K_2 &= 1 + \frac{L_4 + L_9}{2L_2} \end{aligned} \tag{9}$$

In Equation (9), the constant parameters K_0, K_1 and K_2 are the inductors ratios. To calculate the scattering parameter of this cell, we can use M_{12} as follows [25]:

$$S_{21} = \frac{2}{A_1 + B_1/Z_0 + Z_0 C_1 + D_1} \tag{10}$$

Z_0 is the terminals impedance, which will be 50Ω for our triplexer. Using S_{21}, we can obtain the −3dB cut-off angular frequency (ω_C):

$$\begin{aligned} -20 \log |S_{21}(\omega_C)| = -3dB \rightarrow |S_{21}(\omega_C)| = \sqrt{2} \\ \rightarrow |A_1 + B_1/Z_0 + Z_0 C_1 + D_1| = \sqrt{2} \end{aligned} \tag{11}$$

To solve Equation (11), first the imaginary and real sections of S_{21} denominator are extracted as follows:

$$Re\{A_1 + B_1/Z_0 + Z_0 C_1 + D_1\}$$
$$= -\omega^2 L_7 Y_7 Y_6 L_6 (K_0 - \omega^2 L_4 K_1) - \frac{\omega^2 L_7 L_8 Y_7 (K_0 - \omega^2 L_4 K_1)}{50}$$

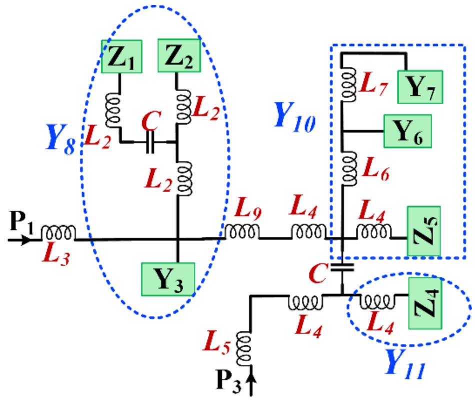

FIGURE 3. Approximated equivalent LC circuit of the BP cell1, where ports 2 and 4 are open.

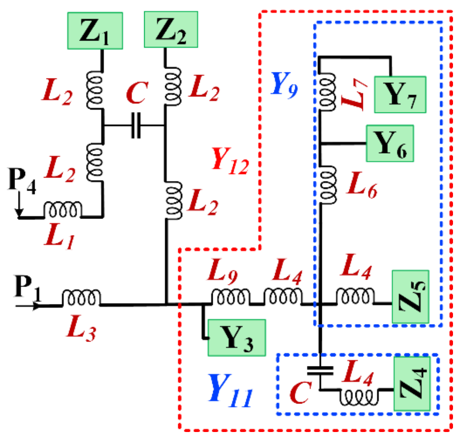

FIGURE 4. Approximated LC model of the BP cell2, where ports 2 and 3 are open.

$$+50(\frac{L_7Y_7}{2L_2} - \omega^2 L_7Y_7L_4K_2) - \omega^2 L_7^2 Y_6^2(\frac{L_6}{2L_2} - \omega^2 L_4L_6K_2)$$
$$Im\{A_1 + B_1/Z_0 + Z_0C_1 + D_1\}$$
$$= \omega L_7Y_7[K_0 - \omega^2 L_4K_1 - \frac{\omega^2 L_7 Y_6^2 L_6 (K_0 - \omega^2 L_4K_1)}{50Y_7}$$
$$+ 50Y_6(\frac{L_6}{2L_2} - \omega^2 L_4L_6K_2) - L_8(\omega^2 L_4K_2 - \frac{1}{2L_2})] \quad (12)$$

As mentioned before, we set T_6 and T_7 as two high impedance lines. Accordingly, Equation (12) will be reduced as follows:

$$Re\{A_1 + B_1/Z_0 + Z_0C_1 + D_1\}$$
$$\approx -\omega^2(L_7Y_7Y_6L_6(K_0 - \omega^2 L_4K_1)$$
$$+ L_7^2Y_6^2(\frac{L_6}{2L_2} - \omega^2 L_4L_6K_2))$$
$$Im\{A_1 + B_1/Z_0 + Z_0C_1 + D_1\}$$
$$\approx 50\omega L_7Y_7Y_6(\frac{L_6}{2L_2} - \omega^2 L_4L_6K_2) \quad (13)$$

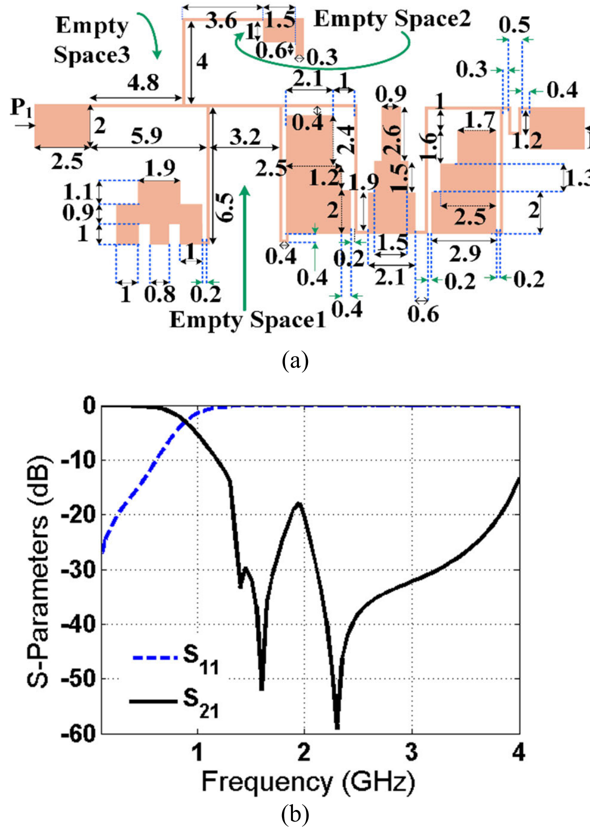

FIGURE 5. Proposed LPF (a) Layout configuration, where all thin lines have 0.1mm widths (unit: mm), (b) frequency response.

A method to solve Equation (13), where ω_C is the cut-off angular frequency is:

$$L_7Y_7Y_6L_6(K_0 - \omega_C^2 L_4K_1) + L_7^2Y_6^2(\frac{L_6}{2L_2} - \omega_C^2 L_4L_6K_2)$$
$$= 0$$
$$\omega_C L_7Y_7Y_6(\frac{L_6}{2L_2} - \omega_C^2 L_4L_6K_2)$$
$$= \frac{\sqrt{2}}{50} \approx 0 \quad (14)$$

In Equation (14), we set the imaginary and real sections of S_{21} denominator equal to $\sqrt{2}$ and zero respectively. By solving Equation (15) we can write:

$$\omega_{C1} = \sqrt{0.5\frac{K_0Y_7 + \frac{1}{2L_2}L_7Y_6}{L_4(K_1Y_7 + K_2L_7Y_6)}}$$
$$\omega_{C2} \approx \sqrt{\frac{1}{2L_2L_4K_2}} \quad (15)$$

where ω_{C1} and ω_{C2} are the cut-off frequencies. Since, we should have only one cut-off frequency, we can use the

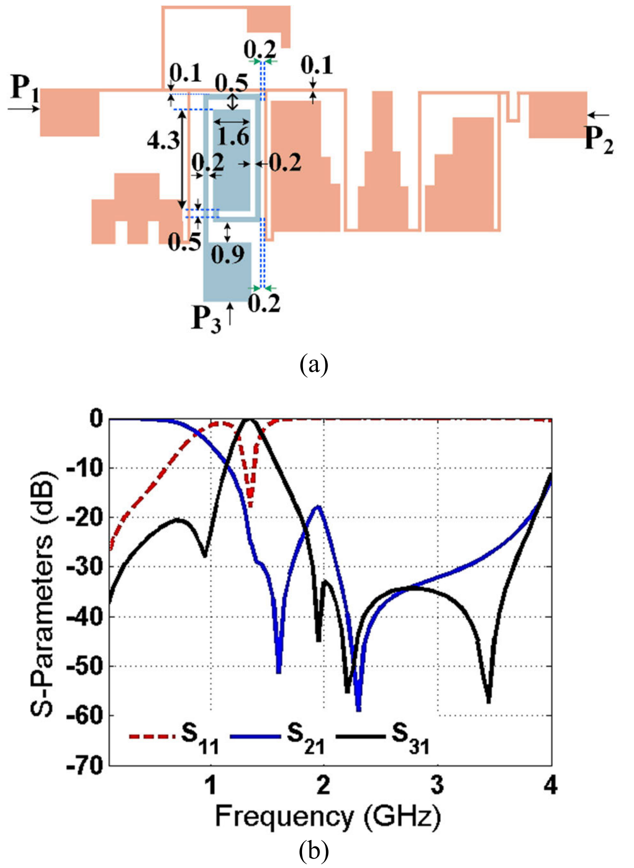

FIGURE 6. Proposed LP-BP diplexer1 (a) Layout and (b) frequency response.

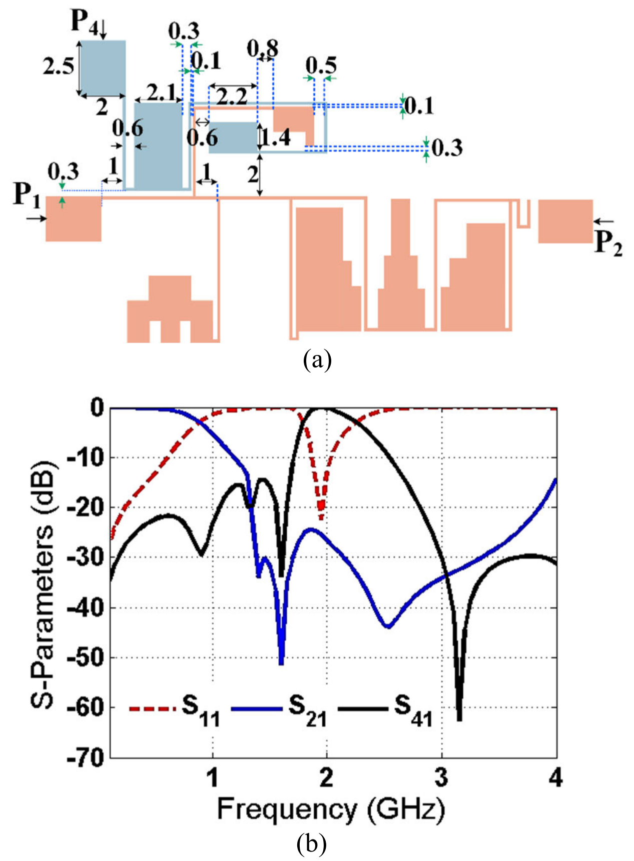

FIGURE 7. Proposed LP-BP diplexer2 (a) Layout and (b) frequency response.

following method to remove the harmonic:

$$\omega_C = \omega_{C1} = \omega_{C2} \rightarrow \frac{K_0 Y_7 L_2 + 0.5 L_7 Y_6}{K_1 Y_7 + K_2 L_7 Y_6} = \frac{1}{K_2}$$
$$\rightarrow 1 + \frac{L_4 + L_9}{2L_2}$$
$$= \frac{(L_3 + (L_4 + L_9)(1 + \frac{L_3}{2L_2}))Y_7 + (1 + \frac{L_4+L_9}{2L_2})L_7 Y_6}{(1 + \frac{L_3}{2L_2})Y_7 L_2 + 0.5 L_7 Y_6} \tag{16}$$

Therefore, we have to tune the values of inductors and admittances in accordance to Equation (16). Based on Equation (16), the LP cell behavior will be determined.

An approximated equivalent LC circuit of the BP cell1, where ports 2 and 4 are open, is shown in Fig.3. When we open P_2, the inductor L_8 will be opened too. As a result, L_1 and L_2 will be open circuited.

The admittance Y_8 is calculated and approximated in Equation (6). The admittances Y_{10} and Y_{11} are derived as follows:

$$Y_{10} \approx \frac{1}{j\omega L_4} \tag{17}$$
$$Y_{11} \approx \frac{1}{j\omega L_4} \tag{18}$$

In Equations (17) and (18), we applied the conditions of having low impedances Z_4 and Z_5. In addition, the admittance Y_6 and the impedance $j\omega L_6$ are high. The transfer matrix between P_1 and P_3 can be calculated as follows:

$$M_{13} = \begin{bmatrix} A_2 & B_2 \\ C_2 & D_2 \end{bmatrix} = \begin{bmatrix} 1 & j\omega L_3 \\ 0 & 1 \end{bmatrix} \times \begin{bmatrix} 1 & 0 \\ \frac{1}{2j\omega L_2} & 1 \end{bmatrix} \times \begin{bmatrix} 1 & j\omega(L_4 + L_9) \\ 0 & 1 \end{bmatrix} \times \begin{bmatrix} 1 & 0 \\ Y_{10} & 1 \end{bmatrix} \times \begin{bmatrix} 1 & 0 \\ j\omega C & 1 \end{bmatrix} \times \begin{bmatrix} 1 & 0 \\ Y_{11} & 1 \end{bmatrix} \times \begin{bmatrix} 1 & j\omega(L_4 + L_5) \\ 0 & 1 \end{bmatrix} \tag{19}$$

After calculations and by substituting Y_{10} and Y_{11}, M_{13} will be obtained (20), as shown at the bottom of the next page.

Using M_{13}, $H_{13}(j\omega)$ (transfer function) can be calculated:

$$H_{1,3}(j\omega_{R1}) = \frac{V_3}{V_1} \rightarrow H_{1,3}(j\omega_{R1}) = \frac{1}{A_2} \quad where\ B_2 = 0 \tag{21}$$

In Equation (21), ω_{R1} is the BP cell1 resonance frequency. The result of substituting A_2 in Equation (21) is:

$$H_{1,3}(j\,\omega_{R1}) = \frac{1}{K_0 + \frac{2K_1}{L_4} - \omega_{R1}^2 CK_1} \quad where\ \ B_2 = 0 \tag{22}$$

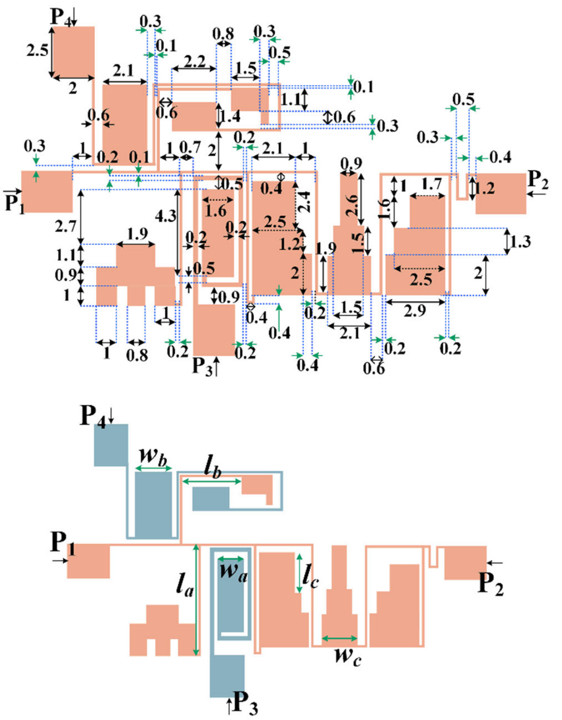

FIGURE 8. Proposed LP-BP triplexer (unit: mm).

The resonance frequency of BP cell1 is at the point where the size of $H_{13}(j\omega)$ becomes one. This condition is presented as follows:

$$\left|H_{1,3}(j\omega_{R1})\right| = 1 \rightarrow \left|K_0 + \frac{2K_1}{L_4} - \omega_{R1}^2 CK_1\right| = 1 \rightarrow$$
$$\omega_{R1,1} = \sqrt{\frac{K_0 + \frac{2K_1}{L_4}}{CK_1}} \tag{23}$$
$$B_2 = 0 \rightarrow$$
$$K_1 + (L_4 + L_5)(K_0 + \frac{2K_1}{L_4} - \omega_{R1}^2 CK_1) = 0$$
$$\rightarrow \omega_{R1,2} = \sqrt{\frac{\frac{K_1}{L_4+L_5} + K_0 + \frac{2K_1}{L_4}}{CK_1}} \tag{24}$$

In Equations (23) and (24), $\omega_{R1,1}$ and $\omega_{R1,2}$ are the BP cell1 resonance frequencies. Because our aim is designing a single-band BPF, one of these frequencies is harmonic and should be removed. A method to get rid of this harmonic is:

$$\omega_{R1,1} = \omega_{R1,2} \rightarrow \frac{K_1}{L_4 + L_5} = 0 \tag{25}$$

This condition leads to $K_1 = 0$ which is not acceptable. Hence, we use the second method. This method is based on moving the harmonic away from the main resonance frequency:

$$\omega_{R1,1} \langle\langle \omega_{R1,2} \rightarrow \frac{K_1}{L_4 + L_5} \rangle\rangle 0$$
$$\rightarrow L_3 + (L_4 + L_9)(1 + \frac{L_3}{2L_2}) \rangle\rangle L_4 + L_5 \tag{26}$$

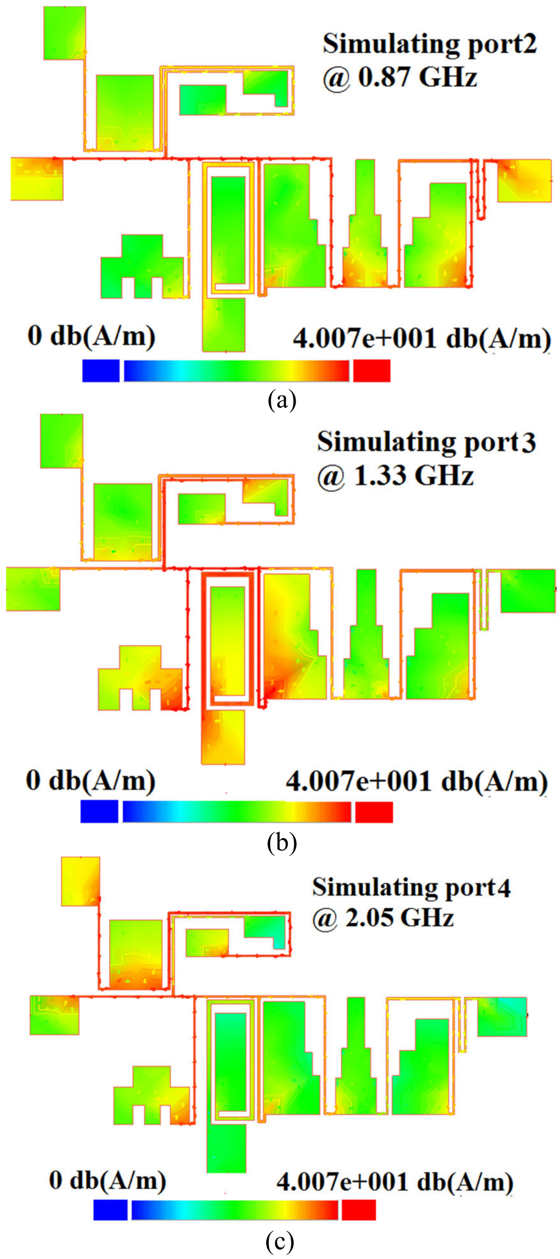

FIGURE 9. Current density distribution simulating (a) port 2 at 0.87 GHz, (b) port 3 at 1.33 GH, (c) port 4 at 2.05 GHz.

$$M_{13} = \begin{bmatrix} A_2 & B_2 \\ C_2 & D_2 \end{bmatrix} \approx \begin{bmatrix} K_0 + \frac{2K_1}{L_4} - \omega^2 CK_1 & j\omega[K_1 + (L_4 + L_5)(K_0 + \frac{2K_1}{L_4} - \omega^2 CK_1)] \\ j\omega[CK_2 - \frac{1}{2\omega^2 L_2} - \frac{2K_2}{\omega^2 L_4}] & K_2 + (L_4 + L_5)(\frac{1}{2L_2} + \frac{2K_2}{L_4} - \omega^2 CK_2) \end{bmatrix} \tag{20}$$

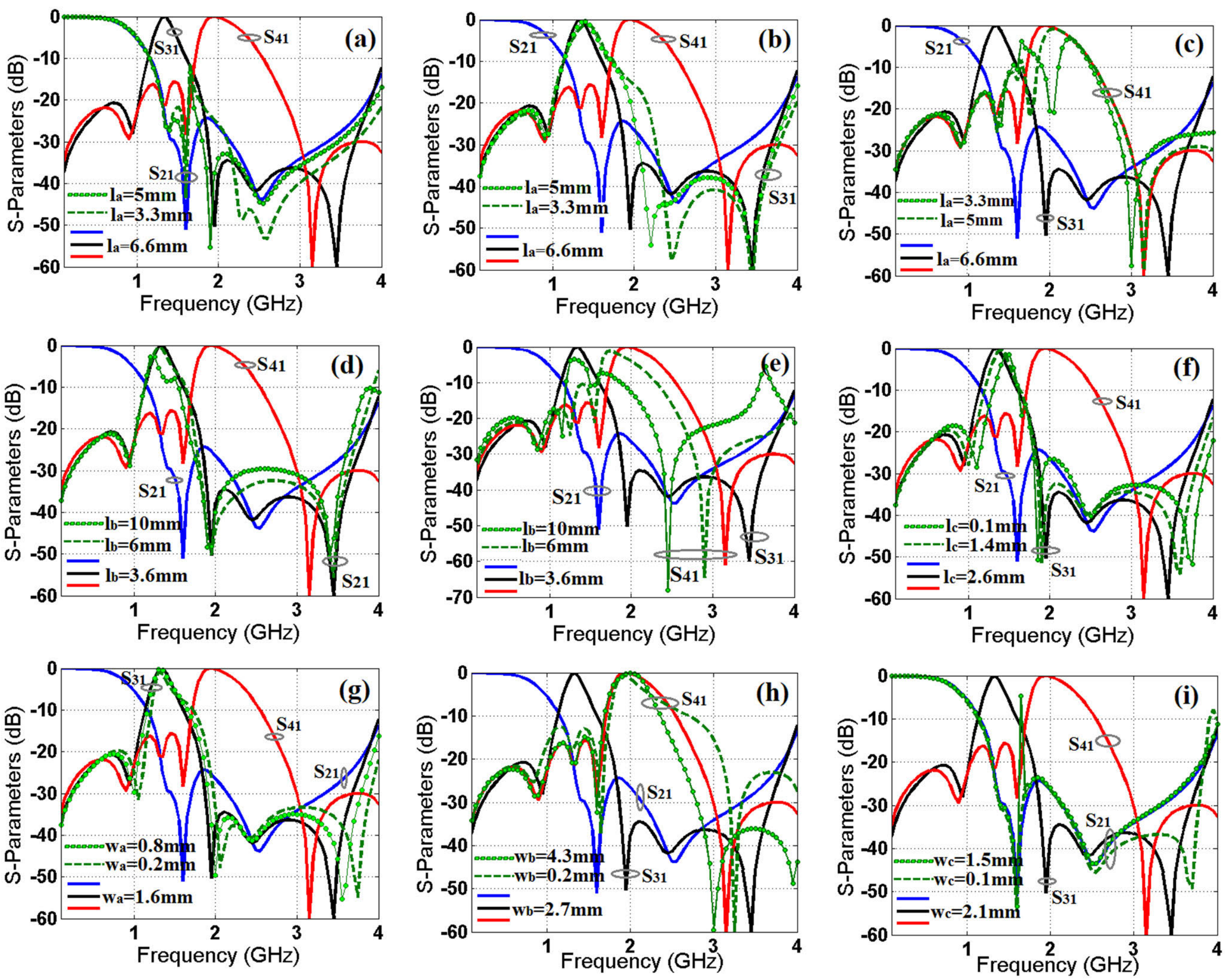

FIGURE 10. Optimization process, (a) S_{21} as a function of l_a, (b) S_{31} as a function of l_a, (c) S_{41} as a function of l_a, (d) S_{31} as a function of l_b, (e) S_{41} as a function of l_b, (f) S_{31} as a function of l_c, (g) S_{31} as a function of w_a, (h) S_{41} as a function of w_b, (i) S_{21} as a function of w_c.

Therefore, to get rid of this harmonic we can tune the inductors in accordance to Equation (26). Design of BP cell 2 (as presented in Fig. 4) is similar to BP cell1.

Using the analyzed basic layout and also optimization a LPF is designed. In Figs.5(a) and 5(b) the frequency response (simulated) and the final layout of this filter are shown. In the design of this filter, some empty spaces are provided for embedding BP cells. The frequency response of the LPF shows that it has a cut-off frequency at 900 MHz with 27.7 dB return loss and 0.1 dB insertion loss. The maximum harmonic level up to 3.9 GHz is −17.85 dB. This filter is simulated on an substrate (h = 0.7874 mm, $\tan(\delta) = 0.0009$ and $\varepsilon_r = 2.22$). This substrate is used for all simulations and the final fabricated triplexer.

By coupling a cell inside the Empty Space 1, LP-BP diplexer1 is obtained and its layout is depicted in Fig.6(a). The dimensions of new sections are written in mm in Fig.6(a). The dimensions of all feeding structures are 2.5mm × 2mm. Fig.6(b) shows the frequency response of diplexer1.

The cut-off frequency of the LP channel and the center frequency of the BP channel are 880 MHz and 1.35 GHz respectively. At this BP channel, the insertion loss is 0.086 dB. Also, its return loss is 24.2 dB. The harmonics of this diplexer are suppressed up to 3.85 GHz with −17.8 dB maximum value.

By coupling another cell inside the Empty Spaces 2 and 3, LP-BP diplexer2 is obtained. The layout of this diplexer is presented in Fig.7(a). Similar to diplexer1, all dimensions are according to the LPF dimensions presented in Fig.5(a). The dimensions of new sections are written in mm, in Fig. 7(a). The dimensions of all feeding structures connected to P_4 is 2.5mm ×2mm. Fig.7(b) shows the diplexer2 frequency response. The cut-off frequency of the LP channel and the center frequency of the BP channel are 880 MHz and 1.95 GHz respectively. Moreover, this BP channel has

TABLE 1. Size and performance comparisons.

Refs.	F_1, F_2, F_3 (GHz)	IL1, IL2, IL3(dB)	RL1, RL2, RL3 (dB)	Δ1%, Δ2%, Δ3%	Selectivity	Size (λg^2/mm^2)	Isolation (dB)	Type
This work	0.87, 1.33, 2.05	0.2, 0.09, 0.04	25.6, 19.4, 25.1	14.1, 25.5	Mediocrity	0.0038/229.6	>19.5	LP-BP Triplexer
[6]	1.85, 3.25, 6.65	0.54, 0.16, 0.55	26.4, 19.9, 19	15, 8.3	Low	0.021/336.4	> 20.5	LP-BP Triplexer
[7]	0.85, 1.6, 2.1	0.72, 1.66, 1.7	16, 13.2, 12.6	13.9, 12.7	Mediocrity	0.048/---	---	LP-BP Triplexer
[8]	1, 2.4, 5.8	0.8, 2.1, 2.5	14.5, 12, 12.9	10, 7	High	---/2940	> 40	LP-BP Triplexer
[9]	0.95, 1.58, 2.8	0.3, 1.16, 2.04	20, 16, 15.4	17, 8.1	Mediocrity	0.018/1126.4	> 32	LP-BP Triplexer
[10]	0.67, 2.15, 3.19	0.55, 0.17, 0.17	14.2, 17.6, 18.08	15, 11.97	Mediocrity	0.006/785	> 20	LP-BP Triplexer
[11]	2.3, 3.2, 3.6	0.78, 1.1, 0.62	19.8, 10, 28	5.2,5.5,1.6	Low	0.095/916	>11.4	BP Triplexer
[12]	2.67, 3.1, 3.43	0.72, 0.63, 0.71	24.5, 24, 24.7	5.2,2.8,9.4	Mediocrity	0.137/997.7	>16	BP Triplexer
[13]	1, 1.25, 1.5	2.7, 1.8, 3.2	Better than 16	9.5,4.2,4.5	High	0.064/2513.7	> 30	BP Triplexer
[14]	1.8 , 3.2, 4.4	1.97, 1.99, 2.3	24, 22, 25	7.4,7.4,6.2	Low	---/1122	> 20	BP Triplexer
[15]	1.65, 2.57	0.047, 0.16	21.8, 20.9	14	High	0.037/722	20	LP-BP Diplexer
[16]	1.88, 3.56	0.12, 0.1	19.2, 36	23.8	High	0.03/303	26	LP-BP Diplexer
[17]	1.46, 2.42	0.68, 0.95	10.2, 16.8	11.13	High	0.037/465	28	LP-BP Diplexer
[18]	2, 3.5	0.3, 1.28	Better than 15	5.5	High	0.093/---	40	LP-BP Diplexer

0.04 dB insertion loss and 24.9 dB return loss. After the BP channel, its harmonics are suppressed up to 3.7 GHz with -24 dB maximum value.

The layout of the final LP-BP triplexer is shown in Fig.8. The triplexer occupies an area of 0.046 λ_g × 0.084 λ_g (11.2 mm × 20.5 mm). The dimensions of the cells that have greater impact on determining the frequency response are shown parametrically by w_a, w_b, l_c, l_a, l_b,and w_c. Internal shunt stubs can be replaced with other large solid stubs with capacitive properties. For example, the solid radial studs can be used instead of the rectangular studs. However, it changes the frequency response slightly.

The current density distributions for simulating Ports 2-4 are presented in Fig.9(a)- Fig.9(c). As illustrated in Fig.9, the thin lines have further current density. For simulating Port 2 at 0.87 GHz, the coupled sections (which are used to create BP channels) have less current density. On the other hand, for simulating Port 3 at 1.33 GHz and Port 4 at 2.05 GHz, the cells used to create LP channel have less current density. The signal passing through port 1 and 2 is a lowpass signal and the role of the coupled cells is weaker. However, for the second and third passbands when ports 3 and 4 are excited, the thin coupled transmission lines play an important role in determining the bandwidths. Therefore, the current density is higher in them.

The frequency response of this triplexer is optimized and a summary of the optimization steps is presented in Fig.10(a)-Fig.10(i). The effects of l_a on S_{21}, S_{31} and S_{41} are depicted in Fig.10(a), Fig.10(b) and Fig.10(c) respectively. Decreasing l_a leads to amplify of harmonics and destroy the second and third bands. However, increasing the length of T-Line with the physical length l_b destroys the BP channels (see Fig.10(d) and Fig.10(e)). As presented in Fig.10(f), increasing the physical length l_c shifts the middle channel to the left. The widths w_a, w_b and w_c can affect the middle, upper and lower channels respectively (see Fig.10(g), Fig.10 (h), and Fig.10(i)). In summary, by using the following steps, we can easily control the bandwidths:

The first step is to find an equivalent LC circuit for our microstrip structure. This includes finding the equivalent inductance and capacitance values for the microstrip components based on their dimensions and material properties. Next, the equivalent LC circuit is used to derive the formulas for the cut-off frequency of the LPF and the resonance frequencies of the BPFs. These formulas are functions of the inductance and capacitance values of the microstrip components. These inductors and capacitors are the equivalents of the physical lengths and widths. Therefore, the effective lengths and widths can be obtained. Finally, utilizing an optimization method to adjust the values of these effective lengths and widths can help to achieve a specified bandwidth.

III. RESULTS, COMPARISON, AND DISCUSSION

The simulations for the proposed LP-BP triplexer are conducted using the Advanced Design System software (EM simulator), with linear steps employed throughout the process. The experimental measurements are done by using an HP8757A. Fig.11(a) and Fig.11(b) display the frequency responses of our triplexer, showcasing the comparison of the simulated and experimental results. In Fig.11(a), the LP band exhibits a cut-off frequency at F_1 = 870 MHz, while the BP channels resonate at frequencies of F_2 = 1.335 GHz and F_3 = 2.055 GHz. The insertion losses for these channels are

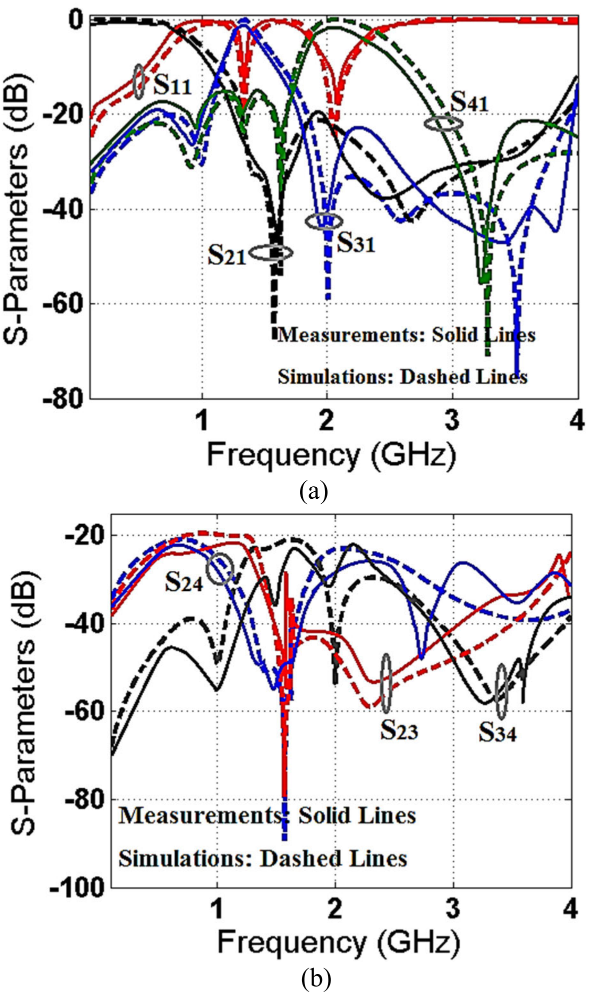

FIGURE 11. Measured and simulated (a) S_{21}, S_{11} and S_{31}, (b) isolations.

recorded at 0.2 dB, 0.09 dB, and 0.04 dB, with the return losses of 25.6 dB, 19.4 dB, and 25.1 dB. Differences between the measured and simulated losses are attributed to factors such as copper and SMA losses, accounting for slightly higher measured values compared to simulations.

The FBW of the second and third bands are 14.1% and 25.5% respectively. As presented in Fig.11(b), the maximum simulated and measured isolations between three channels are $S_{23} = -19.5$ dB, $S_{24} = -20.89$ dB, $S_{34} = -20.98$ dB. To confirm the advantages of our triplexer, a comparison with the previous designs is done in Table 1, where the indexes 1 to 3 mean the 1st to 3rd channels respectively. Also, F, RL, IL and Δ are the operating frequency, return loss, insertion loss and FBW. Since the designed number of this type of triplexers is limited, we had to add the size and performance of some LP-BP diplexers and BP triplexers. From Table 1, it is clear that having low return losses, the most compact size, wide FBWs and the lowest insertion losses at the BP channels are the advantages of this work. Also, the last channel of this triplexer has the widest BP channel in comparison with the previous diplexers and triplexers.

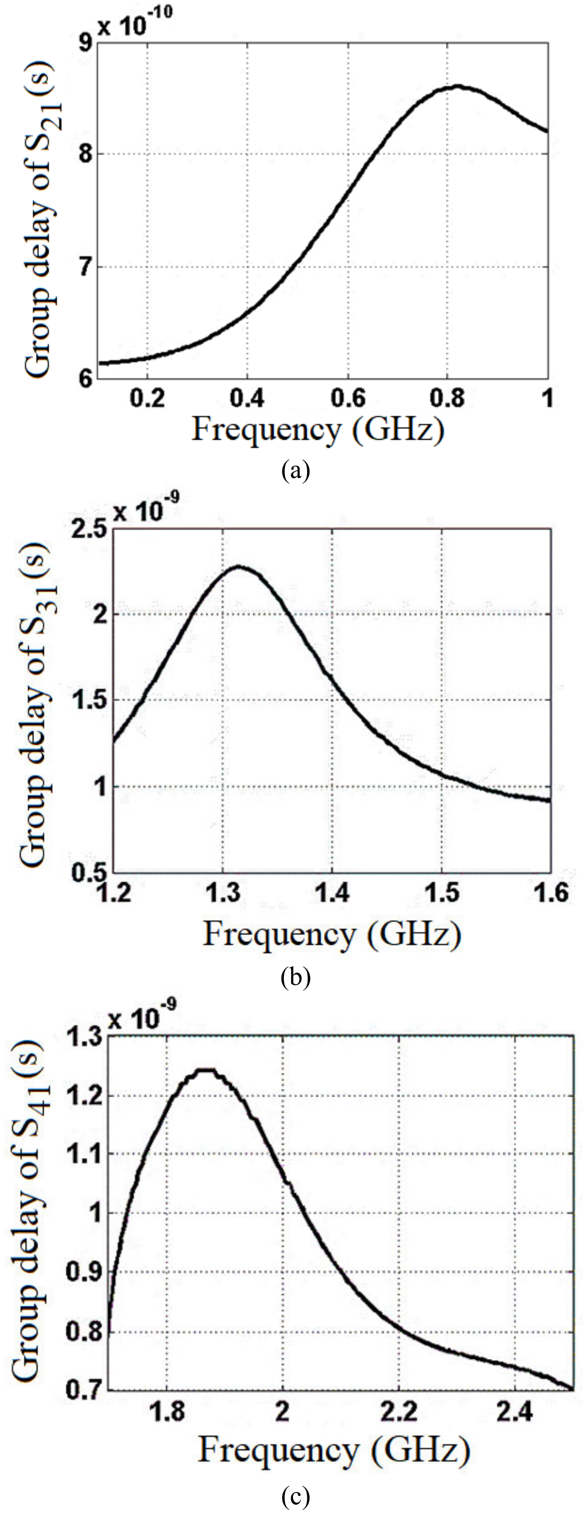

FIGURE 12. GDs of (a) S_{21}, (b) S_{31} and (c) S_{41}.

Among the designed LP-BP triplexers, only in [8] the frequency selectivity is improved significantly. However, it has several problems in terms of large size, high insertion losses and undesired return loss. Group delay (GD) is a key factor in determining the performance for the passive

TABLE 2. GD comparison.

Refs.	Type	Maximum GDs at the Channels (ns)
This work	Triplexer (LP-BP)	0.86, 2.2 , 1.24
[6]	Triplexer (LP-BP)	0.79 , 0.98, 0.85
[8]	Triplexer (LP-BP)	1.5 , 6 , 4.4
[9]	Triplexer (LP-BP)	1.62 , 1.75 , 2.07
[15]	Diplexer (LP-BP)	1.43 , 1.68
[16]	Diplexer (LP-BP)	2 , 1.24
[17]	Diplexer (LP-BP)	0.65, 2.5
[19]	Tri-Channel BPF	< 8 for all bands
[20]	Diplexer (BP-BP)	3.15 , 2.98
[21]	Quad-Channel BP Diplexer	2.76 , 3.31 , 0.91 , 2.15
[22]	Quad-Channel BPF	9 , 6 , 6 , 5
[23]	LPF	5.9
[24]	Dispersive Filter	4.5

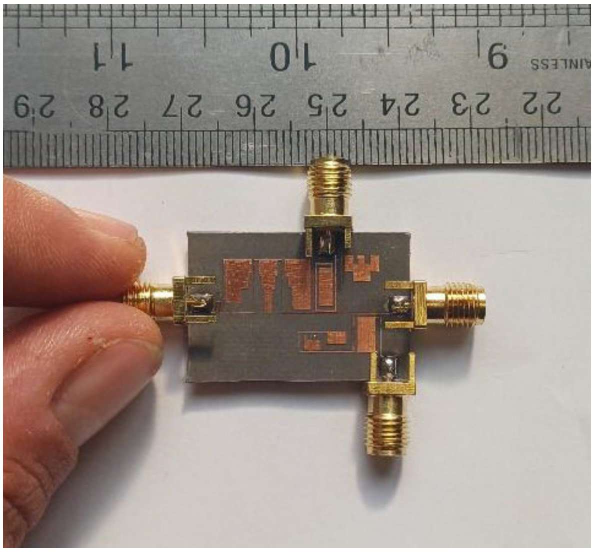

FIGURE 13. Fabricated triplexer.

microstrip structures. However, a few number of reported triplexers pay attention to reduce this factor.

The GDs of scattering parameters are presented in Fig.12(a), Fig.12(b) and Fig.12(c). The GDs of S_{21} (at the lower channel), S_{31} (at the middle channel) and S_{41} (at the upper channel) are 0.86 ns, 2.2 ns and 1.24 ns respectively. These values are acceptable for all wireless networks. The comparison of GDs between this work and the previous ones is presented in Table 2. The presented LP-BP triplexer in [6] has the GDs better than ours. However, the proposed triplexer in [6] is larger than ours. Moreover, our triplexer has lower insertion losses than reference [6].

Also, in [6] the gap between its bands is larger than ours. When the channels are close to each other, obtaining a flat channel with low GD is hard. The development of our microstrip LP-BP triplexer with unique features shows a significant advancement in this field. This triplexer stands out due to its novel structure and remarkable compact size. Furthermore, this triplexer has low loss, wide and flat passbands, low group delay, and compact size simultaneously, a success not achieved by any previous works. Finally, our fabricated triplexer is depicted in Fig.13. As shown in Table 1, the presented designs in [8] and [18] have the best isolation. But our triplexer is smaller and has better insertion and return losses at all channels.

IV. CONCLUSION

Using a novel configuration, a microstrip LP-BP triplexer is designed, analyzed, fabricated and then experimentally measured in this paper. The proposed triplexer highlights excellent performance characteristics, including compact size, flat channels, acceptable group delays (GDs), low insertion losses (ILs), and effective harmonic suppression. The design's suitability for energy harvesting applications makes it a promising solution for various wireless communication systems. Based on its frequency responses, this triplexer is appropriate for low-band and mid-band 5G applications. The design method was based on introducing a semi-layout basic structure and analyzing its approximated LC circuit. Using the analyzed basic structure we could find its behavior, which helped to easy optimization. To prove the superiority of this triplexer, we compared it with the previous designs. Fabrication and measurement results confirm the simulation accuracy, demonstrating the practical feasibility of the proposed triplexer design. Further enhancements and optimizations can be pursued to advance the triplexer's efficiency and applicability in future wireless communication technologies.

REFERENCES

[1] J. Gong, Y. Chen, B. Chen, J. Zhao, K. Xu, Z. Zhong, and M. Liu, "A compact microstrip second-order lossy bandpass filter with improved simplified composite right-/left-handed zeroth-order resonator," *Microw. Opt. Technol. Lett.*, vol. 66, no. 1, Jan. 2024, Art. no. e34015.

[2] L. Nouri, L. Nkenyereye, M. A. Hafez, F. Hazzazi, M. A. Chaudhary, and M. Assaad, "A simplified and efficient approach for designing microstrip bandpass filters: Applications in satellite and 5G communications," *AEU-Int. J. Electron. Commun.*, vol. 177, Apr. 2024, Art. no. 155189.

[3] G. Santra and P. N. Patel, "Designing an omnidirectional horizontally polarized circular patch antenna implementing unequal open-circuited stubs," *Microw. Opt. Technol. Lett.*, vol. 66, no. 1, Jan. 2024, Art. no. e34014.

[4] R. H. Elabd, A. J. A. A. Gburi, and J. Alsayaydeh, "An ultra-selective OLR-based microstrip diplexer with minimal insertion loss for wireless communication system," *Int. J. Intell. Eng. Syst.*, vol. 17, no. 2, pp. 83–94, 2024.

[5] A. Rezaei, S. I. Yahya, and L. Nouri, "An ultra-compact diplexer based on simple microstrip coupled lines for GSM and wideband wireless applications," *Wireless Netw.*, vol. 30, no. 2, pp. 857–865, Feb. 2024.

[6] L. Nouri, S. I. Yahya, A. Rezaei, F. Hazzazi, M. A. Chaudhary, M. Assaad, and B. N. Nhu, "Microstrip lowpass-bandpass triplexer with flat channels and low insertion losses: Design and fabrication for multi-service wireless communication systems," *AEU-Int. J. Electron. Commun.*, vol. 170, Oct. 2023, Art. no. 154807.

[7] C. Zhu, J. Xu, W. Kang, and W. Wu, "Design of balun-integrated switchable low-pass-bandpass triplexer," *IEEE Microw. Wireless Compon. Lett.*, vol. 27, no. 4, pp. 353–355, Apr. 2017.

[8] F.-C. Chen, J.-M. Qiu, H.-T. Hu, Q.-X. Chu, and M. J. Lancaster, "Design of microstrip lowpass-bandpass triplexer with high isolation," *IEEE Microw. Wireless Compon. Lett.*, vol. 25, no. 12, pp. 805–807, Dec. 2015.

[9] J. Xu, Z.-Y. Chen, and H. Wan, "Lowpass–Bandpass triplexer integrated switch design using common lumped-element triple-resonance resonator technique," *IEEE Trans. Ind. Electron.*, vol. 67, no. 1, pp. 471–479, Jan. 2020.

[10] L. Nouri, F. Zubir, L. Nkenyereye, A. Rezaei, M. Abdel-Hafez, F. Hazzazi, M. A. Chaudhary, M. Assaad, and Z. B. Yusoff, ''Novel ultra-compact wide stopband microstrip lowpass-bandpass triplexer for 5G multi-service wireless networks,'' *IEEE Access*, vol. 12, pp. 2926–2940, 2024, doi: 10.1109/ACCESS.2023.3348786.

[11] A. Rezaei, S. I. Yahya, L. Noori, and M. H. Jamaluddin, ''Design and fabrication of a compact microstrip triplexer for Wimax and wireless applications,'' *Eng. Rev.*, vol. 41, no. 1, pp. 85–91, 2020.

[12] A. Rezaei and L. Noori, ''Novel low-loss microstrip triplexer using coupled lines and step impedance cells for 4G and Wimax applications,'' *TURKISH J. Electr. Eng. Comput. Sci.*, vol. 26, no. 4, pp. 1871–1880, Jul. 2018.

[13] C.-F. Chen, T.-M. Shen, T.-Y. Huang, and R.-B. Wu, ''Design of multimode net-type resonators and their applications to filters and multiplexers,'' *IEEE Trans. Microw. Theory Techn.*, vol. 59, no. 4, pp. 848–856, Apr. 2011.

[14] A. Chinig, A. Errkik, L. E. Abdellaoui, A. Tajmouati, J. Zbitou, and M. Latrach, ''Design of a microstrip diplexer and triplexer using open loop resonators,'' *J. Microw., Optoelectron. Electromagn. Appl.*, vol. 15, no. 2, pp. 65–80, Jun. 2016.

[15] A. Rezaei, S. I. Yahya, and L. Nouri, ''Design and analysis of a compact microstrip lowpass–bandpass diplexer with good performance for wireless applications,'' *Int. J. Microw. Wireless Technol.*, vol. 15, no. 7, pp. 1099–1107, Sep. 2023.

[16] M. Hayati, A. Rezaei, and L. Noori, ''Design of a high-performance lowpass–bandpass diplexer using a novel microstrip structure for GSM and WiMAX applications,'' *IET Circuits, Devices Syst.*, vol. 13, no. 3, pp. 361–367, May 2019.

[17] M. Hayati, A.-R. Zarghami, S. Zarghami, and S. Alirezaee, ''Designing a miniaturized microstrip lowpass-bandpass diplexer with wide stopband by examining the effects between filters,'' *AEU-Int. J. Electron. Commun.*, vol. 139, Sep. 2021, Art. no. 153912.

[18] S. Elden and A. K. Gorur, ''Design of a compact lowpass-bandpass diplexer with high isolation,'' *Prog. Electromagn. Res. Lett.*, vol. 97, pp. 21–26, 2021.

[19] Y. Liu, ''A tri-band bandpass filter realized using tri-mode T-shape branches,'' *Prog. Electromagn. Res.*, vol. 105, pp. 425–44, 2010.

[20] H. Heshmati and S. Roshani, ''A miniaturized lowpass bandpass diplexer with high isolation,'' *AEU-Int. J. Electron. Commun.*, vol. 87, pp. 87–94, Apr. 2018.

[21] L. Nouri, S. Yahya, and A. Rezaei, ''Design and fabrication of a low-loss microstrip lowpass-bandpass diplexer for Wimax applications,'' *China Commun.*, vol. 17, no. 6, pp. 109–120, Jun. 2020.

[22] A. Rezaei, L. Noori, and M. H. Jamaluddin, ''Novel microstrip lowpass-bandpass diplexer with low loss and compact size for wireless applications,'' *AEU-Int. J. Electron. Commun.*, vol. 101, pp. 152–159, Mar. 2019.

[23] M. Hayati, M. Ekhteraei, and F. Shama, ''A compact microstrip lowpass filter with flat group-delay and ultra high figure-of-merit,'' *Appl. Comput. Electromagn. Soc. J. (ACES)*, vol. 32, no. 2, pp. 147–152, 2017.

[24] E. Avignon-Meseldzija, J. Anastasov, and D. Milic, ''A linear group delay filter with tunable positive slope for analog signal processing,'' *Int. J. Circuit Theory Appl.*, vol. 49, no. 5, pp. 1307–1326, May 2021.

[25] J. S. Hong and M. J. Lancaster, *Microstrip Filters for RF/Microwave Applications*. New York, NY, USA: Wiley, 2001.

SALAH I. YAHYA (Senior Member, IEEE) received the B.Sc. degree in electrical engineering, the M.Sc. degree in electronics and communication engineering, and the Ph.D. degree in communication and microwave engineering. He is a Consultant Engineer and a Senior Member of USA and AMTA-USA. He has many published research articles in high quality journals and he has presented many conference papers. His research interests include antenna design, numerical RF dosimetry, MW measurement, and MW components design. He has been a regular reviewer of the Electromagnetics Academy, Cambridge, USA, PIERS journals publications, *Science and Engineering of Composite Materials* and *International Journal of Applied Electromagnetics and Mechanics*, since 2009.

FARID ZUBIR (Member, IEEE) received the B.Eng. degree in electrical (majoring in telecommunication) and the M.Eng. degree in RF and microwave from Universiti Teknologi Malaysia (UTM), in 2008 and 2010, respectively, and the Ph.D. degree from the University of Birmingham, U.K., in 2016, for research into direct integration of power amplifiers with antennas in microwave transmitters. He is currently an Assistant Professor with the Department of Communication Engineering, Faculty of Electrical Engineering, UTM. In 2019, he was an Honorary Postdoctoral Research Fellow with The University of British Columbia (UBCO), Okanagan, Canada, for two years, where he has conducted research into highly efficient and linear amplification power amplifier topology for wireless power systems. His research interests include RF and microwave technologies, including planar array antennas, dielectric resonator antennas (DRA), and active integrated antennas (AIA).

LEWIS NKENYEREYE received the Ph.D. degree in information security from Pukyong National University, Busan, South Korea. He was a Research Fellow with the Creative Human Resource Development Program for IT Convergence, Pusan National University. He was a Visiting Scholar with Thompson Rivers University, Kamloops, BC, Canada, and Georgia Southern University, Statesboro, GA, USA. He is currently an Assistant Professor of computer and information security with the Department of Computer and Information Security, College of Electronics and Information Engineering, Sejong University, Seoul, South Korea. His research spans across the wide range of security and privacy related techniques with a particular interest in the Internet of Things (specifically the Internet of Vehicles). He is also involved in privacy-preserving techniques projects for blockchain-based applications and interoperability challenges in the IoT and M2M standards (with a special focus on one M2M). He has served as a member of several technical program committees in various conferences and journals.

MOHAMMED ABDEL HAFEZ (Senior Member, IEEE) received the B.Sc., M.Sc., and Ph.D. degrees in electrical and electronic engineering from Eastern Mediterranean University (EMU), Northern Cyprus, Turkey, in June 1992, August 1994, and November 1997, respectively. From 1992 to 1997, he was a Research Engineer with the Department of Electrical and Electronic Engineering, EMU. In 1995, he was an Instructor with the Department of Electrical Engineering, Al-Quds University. From 1997 to 1999, he was a Senior Manager with on Manager with Palestine Telecommunication Company. In August 1999, he joined the Centre for Wireless Communications, University of Oulu, Oulu, Finland, as a Senior Research Scientist and the Project Manager. He is an Associate Professor of electrical and communication engineering with United Arab Emirates University, United Arab Emirates. He is also a frequent Visiting Scientist with the Centre for Wireless Communications, University of Oulu. His research interests include modeling, design, and performance analysis of wireless communication systems; radio access; sensor networks; the IoT; cooperative and relay networks; NOMA; cognitive radio networks; advanced receivers' algorithms; and ultra-wideband (UWB) communication.

LEILA NOURI received the B.Sc. and M.Sc. degrees in electronic engineering from Razi University, Kermanshah, Iran, in 2005 and 2009, respectively, and the Ph.D. degree in electronic engineering from the Shiraz University of Technology. She is the author of one books, more than 60 articles, and more than five research and industrial projects. Her research interests include microstrip coupler, microstrip filter, neural networks, and LNAs.

MAHER ASSAAD received the master's degree in electrical engineering/microelectronics IC design from the University of Montreal, Montreal, Canada, in 2002, and the Ph.D. degree in electrical engineering/microelectronics IC design from the University of Glasgow, Glasgow, U.K., in 2009. He was a Senior Lecturer of electrical engineering with the University Technology of PETRONAS, Malaysia, and an Associate Professor of electronic and communication engineering with American University of Ras Al Khaimah, United Arab Emirates. He is currently a Professor of electrical and computer engineering with Ajman University, United Arab Emirates. His research interests include the design of circuits/integrated circuits for various type of sensors and wireline and optical communication systems.

MUHAMMAD AKMAL CHAUDHARY (Senior Member, IEEE) received the master's and Ph.D. degrees in electrical and electronic engineering from Cardiff University, Cardiff, U.K., in 2007 and 2011, respectively, and the M.B.A. degree in leadership and corporate governance from Edinburgh Business School, Heriot-Watt University, Edinburgh, U.K., in 2022. Before joining Ajman University, United Arab Emirates, in 2012, he held a postdoctoral research position with the Centre for High-Frequency Engineering, Cardiff University. He is currently an Associate Professor of electrical engineering with Ajman University. His research interests include nonlinear device characterization, spectrum-efficient power amplifiers, nonlinear measurement techniques, and microwave electronics have resulted in more than 100 academic articles. He is a Chartered Engineer of the Engineering Council, U.K., and a fellow of the Higher Education Academy, U.K.

NOORLINDAWATY MD. JIZAT (Member, IEEE) received the B.E. and M.S. degrees in electrical engineering (telecommunication) from Universiti Teknologi Malaysia (UTM), in 2008 and 2010, respectively. She is currently pursuing the Ph.D. degree in electrical engineering (telecommunication) with Multimedia University (MMU), Malaysia. From 2008 to 2012, she was a Quality Engineer with Flextronics Technology Sdn Bhd; and a Research and Development Engineer with Panasonic System Network Malaysia. She is a Lecturer with the Faculty of Engineering, Multimedia University. Her research interests include beamforming networks, Butler Matrix, beam steering, antenna array, self-powered solar Wi-Fi systems, and material research into antenna applications.